ACTA TECHNICA CORVINIENSIS – Bulletin of Engineering
Tome VI (Year 2013) – FASCICULE 4 [October–December]
ISSN 2067–3809

[1.] Liany Amelia HENDRATTA, [2.] Terunori OHMOTO

RESISTANCE AND FLOW CHARACTERISTICS OF HIGH-CONCENTRATION SEDIMENT LADEN FLOW OVER DUNE TYPE BED IN AN OPEN CHANNEL

[1.] DEPARTMENT OF CIVIL AND ENVIRONMENTAL ENGINEERING, KUMAMOTO UNIVERSITY, JAPAN

ABSTRACT: The need to understand and predict flows that carry large loads of suspended sediments and wash loads has become acute in the Yellow River Basin, where significant erosion and siltation associated with high-concentrated floods produce significant erosion, siltation, and associated river problems. Mud flows, debris flows and slurries, which contain large concentrations of clay and/or silt particles suspended in water, often show non-Newtonian hydrodynamic properties. Non-Newtonian flows are poorly understood regarding the impact of their rheological properties on fully developed turbulent flows. In this paper, we experimentally investigated resistance and flow structure of high-concentrated sediment laden flow in an open channel using particle image velocimetry. The results showed that, compared with clear water flow, the rheological properties of sediment-laden flow significantly dissipated the turbulent flow fluctuations over the dune type bed and increased the flow resistance.
KEYWORDS: non-Newtonian fluid, mudflows, dune type bed, particle image velocimetry

INTRODUCTION

Waves in rivers and artificial channels are commonly caused by sand and pebbles from the base. Changes in beds and river channels occur as a result of sediment transport and that morphology influences the flow structures such as resistance law. Sand waves, which change with the characteristics of the riverbed material and water utilization conditions, have a close relationship with the flow-resistance, suspended sediment, and river bed fluctuation. Therefore, the studies of sand waves are one of the basic issues of sediment hydraulics. Various phenomena, concerning eddy of structure and sediment transport, seen in actual rivers have a strong relationship with riverbed forms. Thus, the investigation of how sand waves influence flow distribution has been the focus of strong interest among numerous researchers and engineers for years. Observing the riverbed material reach the surface of the river, Matthes (1947) predicted that a strong water spout-like rising eddy exists. From the observation of the Brahmautra river in the East Pakistan, where long term flooding occurs, Coleman (1969) pointed out that a cork boiling eddy is generated from the trough of the dune. It is difficult to grasp the organizational structure of the turbulent underwater flow in the real river. Therefore, experiments that imitate the real phenomena in the laboratory have been prevalent. Utami and Ueno (1977) conducted a visualization experiment under bed conditions that are likely to create a buoyantly rising eddy and explained the large scale characteristics of an eddy motion in an observation with a horseshoe-shaped eddy model. Ikeda and Aseada (1983) measured suspended sediment concentration of riverbed waves in the flow of the moving bed and suggested a strong relationship between suspended sediment concentration and riverbed configuration associated with the rising eddy. Yazu (1997) argued that it is possible to conduct an observation with a laser velocimeter and the hydrogen bubble method and use spatiotemporal correlational analysis to explain the eddy of structure that are formed behind the continuous sand waves with a horseshoe-shaped eddy model from the standpoint of cross sectional characteristics and three dimensionality.

Hayashi et al. (2002) conducted numerical experiment that applied the Direct Numerical Simulation (DNS) on open-channel flow with sand bank waves and demonstrated that the detection and visualization of the tubular swirling eddy can lead to the generation of reverse horseshoe-shaped eddy, a horseshoe-shaped eddy with the top and bottom of the "horseshoe" turned upside down. However, these studies used either clear water flow or low density flow. The study that focused on the relationship between high density flow such as the one observed in the Yellow River and sand waves is scarce. One of the biggest obstacles when conducting an experimental study under the high density flow conditions involves the difficulty of the measurement. It is impossible to clarify the flow structure by means of a Pitot tube current meter used in the past or the measurement of the concentration distribution.

Regarding the resistance of hyperconcentrated sediment-laden flows, it has been reported that in an experiment conducted by using silt specimens with a median grain size (d_{50}) of 0.026 mm, resistance tended to decrease as sediment concentration increased. (Yang,C.T. and X.Kong,1991), It has also been reported, however, that in an experiment conducted by Wang (1993) by using clay, resistance increased slightly at a volume concentration of about 9%.

Paying attention to non-Newtonian fluid properties of high-concentrated sediment flows, Ohmoto T. and Cui Z. (2005), conducted an experiment in which high-concentrated sediment flow was artificially generated in pipe flow by using bed material samples taken in Jinan City, China, in a lower reach of the Yellow River and commercially available clay (kaolin) and investigated their resistance properties. Both in the Yellow River sediment case and in the kaolin case, the friction loss coefficient increased as sediment concentration increased. At the volume concentration of 10%, the friction loss coefficients of the Yellow River sediment and kaolin were greater than the friction loss coefficient of clear water flow by factors of 1.30 and 1.28, respectively, indicating a slightly greater value for the Yellow River sediment

In the present study we took advantage of the sodium polyacrylate (PSA) solution that resembles high-concentration sediment in viscosity characteristics to thoroughly consider the impact of sediment concentration on resistance characteristics of the dune-type beds and flow structures in the drug-reducing flow. Particle image velocimetry (PIV) was applied to current meters to compare clear water flow with the flow field over a fixed wavy bed that mimicked a dune-type bed. This study deals only with wash loads when considering high-concentrated sediment-laden flows and assumes that fine-grained sediment is not deposited on the channel bed, and spatial changes in concentration distribution are small. To investigate resistance characteristics, artificial flow was created with the PSA solution through fixed wavy bed in open channels that mimicked dune. We examined flow mechanism of the high-concentrated sediment laden flow over dune-type beds of open channels with the PSA solution as stimulant fluid.

EXPERIMENTAL APPARATUS AND METHODS

For the measurement of viscosity, Brookfield's DV-II +PRO digital viscometer was used. The DV-II viscometer is a coaxial cylinder type rotational viscometer that excels in low-viscosity and low-shear-rate measurement. Temperature control can be adjusted by connecting a well-insulated tube from the circulation-type temperature-controlled water tank capable of controlling water temperature at accuracy of ±0.3°C to the viscometer.

The materials used for viscosity measurement are suspensions of the Yellow River sediment, suspensions of kaolin and sodium polyacrylate (PSA) solutions used as polymer solutions. The Yellow River sediment used is bed material sampled at the Kuokou hydrometric station (278 km upstream from the river mouth) in Jinan City located in a lower reach of the Yellow River. The Yellow River sediment had a median grain size of d_{50} = 16.4 μm and a density of ρ_s = 2.68 g/cm^3, while the kaolin had a median grain size of d_{50} = 5.3 μm and a density of ρ_s = 2.7 g/cm^3.

The kaolin suspensions and PSA solutions used in the viscosity experiment were made to flow in a circulating variable-slope flume made of acrylic resin measuring 10 m in length, 0.4 m in width and 0.2 m in height. The experiment conditions are shown in Table 1. Resistance was calculated by measuring water depth of a uniform flow field with gauges point. In order to simulate a continuous dune bed, we installed 80 waves in the direction of downward flow between the space of 6.4m from the upper reach of the channel. Although each wave length and each wave-height of the dune may seem varied, on average both wave length and wave-height demonstrate strong correlations with depth. The wave length is about five times the value of the depth while wave-height ranges between 1/4 to 1/3 of the depth. In this experiment the wave length and wave height were established at λ = 8 cm and h_s = 1 cm, respectively. The dimensionless wave height h_s /H and dimensionless wave length λ/H relative to the water depth H are about 1/3 and 3, respectively. Thus, wave length is somewhat short. The dune is more or less two dimensional in planar form and has transversely uniform ridges and valleys.

Table 1. Experimental conditions

	Clear water	PSA solution (800mg/l)
Flow rate Q(l/s)	1.7	1.7
Flow depth H(cm)	2.5	3.5
Mean flow velocity U_m(cm/s)	17.0	12.1
Maximum velocity U_0(cm/s)	20.8	18.0
Gradient of channel i0	1/2000	1/2000
Froude number Fr	0.34	0.21
Reynolds number Re	4250	

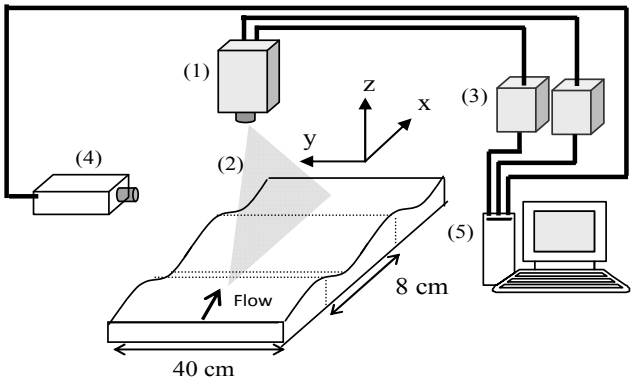

(1) Double-pulsed LASER Illumination System
(2) Laser sheet
(3) YAG - Laser Main unit
(4) CCD- Camera Kodak Megaplus ES1.0
(5) P.C.with Visi flow-software (Timing control and analyze)

Figure 1. Particle image velocimetry (PIV) measurement system

Figure 1 illustrates the measuring system used in the present study. The origin of the coordinate system was located at the midpoint of a dune ridge 2 m downstream from the upstream end of the flume. The x, y and z axes were defined as the streamwise direction, the transverse direction and the vertical

direction, respectively, and their velocity fluctuation components were defined as u, v and w. We used air-cooled double pulsed YAG laser as a light source for PIV. The sheet light was adjusted to 1mm in thickness, 10cm in width, and 1000μsec in pulse interval. We transmitted the light vertically downward from the upper channel to the bottom. We captured the two visualized images of the particle passing through the laser sheet with the CCD camera (Kodak Megaplus ES1.0 : 1008×1008 pixel) installed at the side of the channel. The particle image velocimetry (PIV) was measured between the interval of one wavelength at the point 2m from the upper reach of the channel. Sampling frequency for flow velocity was 15Hz. Statistical analysis was conducted with the 1000 samples of image data per one measurement site. The present experiment investigated the effects of changes in PSA concentration on resistance characteristics and the resistance laws of the flow at fixed concentration. Nylon particles 5 μm in diameter and having a specific gravity of 1.02 were used as tracers.

EXPERIMENTAL RESULTS - Viscous properties

Figures 2 and 3 show the shear rate dependence of shear stress and the apparent viscosity of high-concentrated sediment suspensions and PSA solutions. Shear stress and the apparent viscosity of a PSA solution is linearly related to the shear rate on log-log paper. This indicates that a PSA solution and a hyper-concentrated sediment suspension have similar viscous properties.

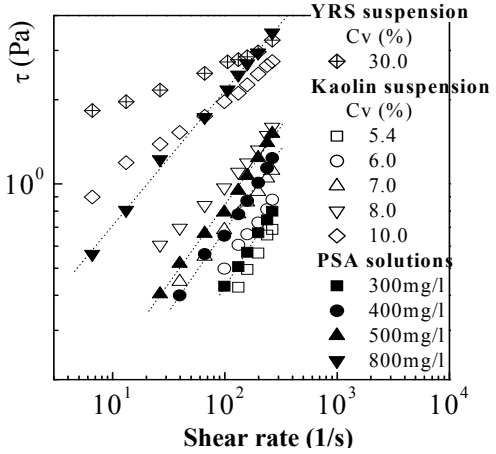

Figure 2. Relation between shear stress and shear rate

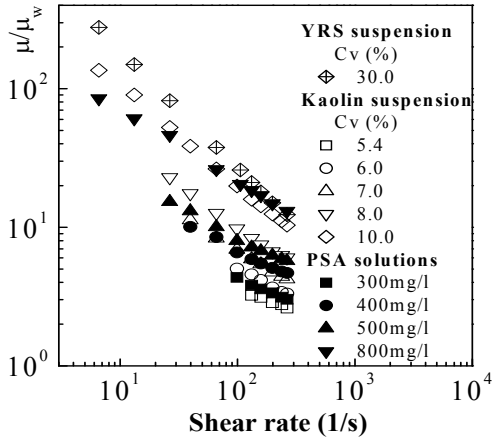

Figure 3. Relation between viscosity and shear rate

Figure 4 shows the shear rate dependence of the kinematic viscosity of kaolin suspensions and the kinematic viscosity of PSA solutions. As shown, the kinematic viscosities of the PSA solutions at concentrations of 300 mg/l, 400 mg/l, 500 mg/l and 800 mg/l are close to the kinematic viscosities of the kaolin suspensions at volumetric concentrations (C_v) of 6%, 7%, 8% and 10%, respectively. This indicates that the PSA solutions have non-Newtonian fluid properties affects the apparent viscosity.

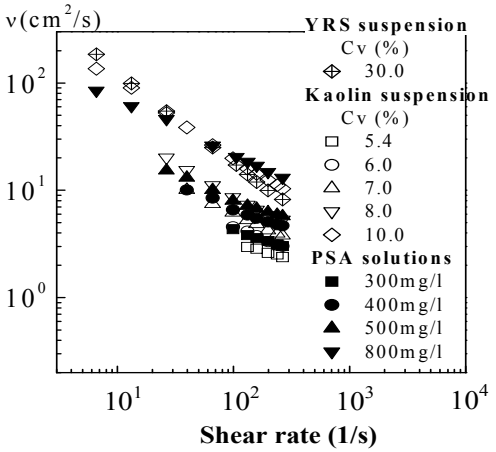

Figure 4. Relation between kinematic viscosity and shear rate

Resistance properties

Figure 5 shows the relationship between the total resistance coefficient and PSA solution concentration.

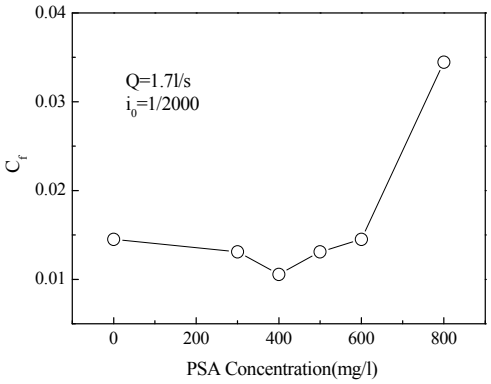

Figure 5. Relationship between the total resistance coefficient and PSA solution

The total resistance coefficient, which is defined as the ratio between the inertia force of a fluid and the total resistance calculated as the sum of friction resistance and form resistance, can be expressed as

$$C_f = 2\left(\frac{U}{U_M}\right)^2 \qquad (1)$$

where $U_* = (g\, h_m\, i_0)^{1/2}$; g, gravitational acceleration; i_0, the slope of the flume; U_m, section-averaged flow velocity. The total resistance coefficient C_f decreases to PSA400mg/l (7% sediment concentration) with the thickness in the PSA concentration, up to 27% compared to that of the clear water and tends to increase again from that point. In the PSA800mg/l solution case (10% sediment concentration) the resistance can increase about 146% of that of the clear water. This tendency for resistance to decrease with the increase in the thickness of the concentration to a certain point until it starts to increase has been observed in a smooth open channel

by Ohmoto et al. (2012). In contrast to the simplicity of the flow over the smooth open channels, this is one of the characteristics of the high density flow that exists under the complicated boundary condition.

Average flow characteristics

Figure 6 shows isolines of a stream function Ψ defined by Eq. (2).

$$\psi(x,z) = \int_0^z U(x,\zeta)d\zeta \qquad (2)$$

where U represents a time-averaged flow velocity. As demonstrated in the Figure reattachment point in the in the clear water case was at x/hs=3.5. Furthermore, circulating flow was detected near the substratum of the separation line. However, in the PSA800mg/l case the circulating zone with Ψ smaller than 0 was identified in the vicinity of the base behind the ridge. The location of the reattachment point was not clearly acknowledged due to the extremely small size of the region.

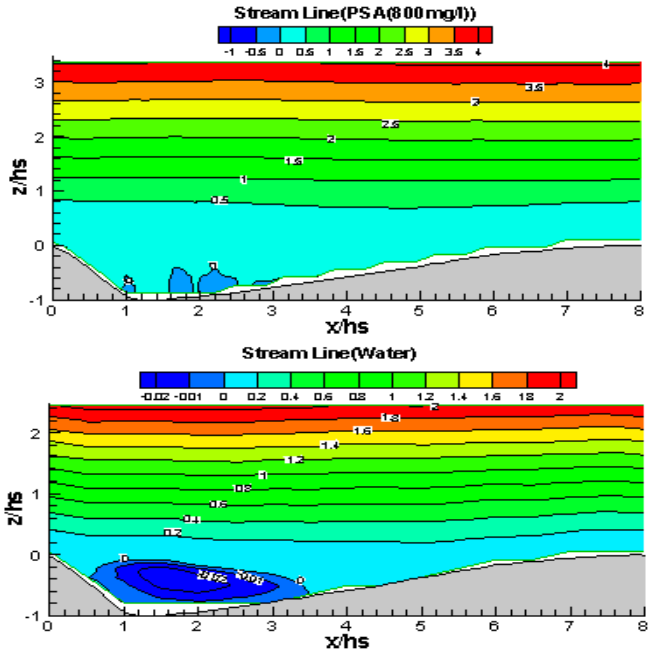

Figure 6. Isolines of a stream function

Figure 7 shows the vertical distribution of main flow velocity changes in the flow direction over a dune-type bed in the clear water case and the PSA solution case. The vertical and horizontal axes were made dimensionless by dune wave height h_s. The flow velocity scale was made dimensionless by the maximum over-ridge flow velocity U_0. The vertical axis is shown at intervals of x/hs = 0.5 in the flow direction. In the PSA 800mg/l solution case, the range in which the rate of change for main flow velocity in the vertical direction is high, has been approximated with a straight line. The vertical distribution of main flow velocity shows characteristics of a free mixing layer behind a ridge, suggesting the growth of an internal boundary layer along the bed surface further downstream and the influence of flow acceleration due to the forward pressure gradient. Compared to the clear water case, flow separation and the resultant development of circulation flows are not pronounced in the PSA solution case. It is interesting to note that in the PSA solution case, unlike in the clear water case, there are two clearly-discernible high-shear-rate areas. The solid line in the clear water case indicates the flow separation line.

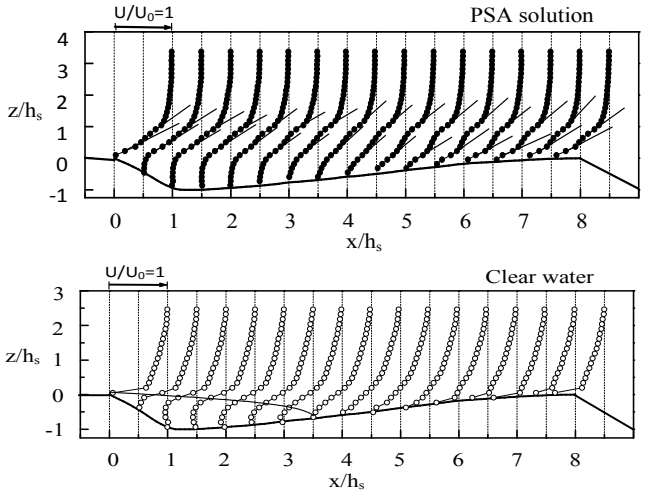

Figure 7. Vertical distribution of main flow velocity

Turbulence characteristics

Figure 8 demonstrates how downward flow and vertical flow directions influence the vertical distribution of turbulence intensity and changes in the streamwise direction.

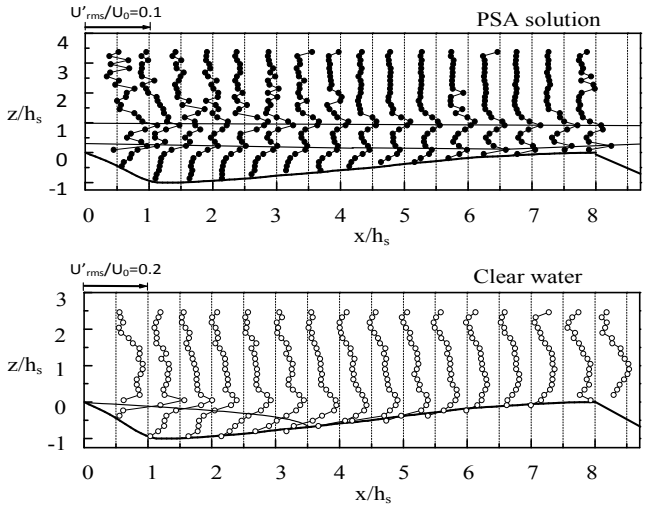

Figure 8. Vertical distribution of turbulence intensity

The solid lines in the figures were drawn to connect the maximum values of turbulence intensity at different flow distances. In the PSA solution case, the maximum values of turbulence intensity are identified at two height levels, namely, z/h_s = 1 and z/h_s = 0.2 to 0.3, both in the streamwise direction and in the vertical direction. In the clear water case, turbulence intensity tended to increase in the deceleration region from the upstream ridge to the reattachment point and decreased considerably near the bed surface in the acceleration region from z/h_s = 4 to the downstream ridge. Compared to the clear water case, in the PSA 800mg/l solution case, turbulence intensity decreased to about 50% in the streamwise direction and about 30% in the vertical direction relative to the clear water case. In the vertical distribution of turbulence intensity in the PSA solution case, the maximum values occurred at two locations under the influence of flow separation and shear deformation of the internal boundary layer

of the bed. This greatly differs from what was observed in the clear water case.

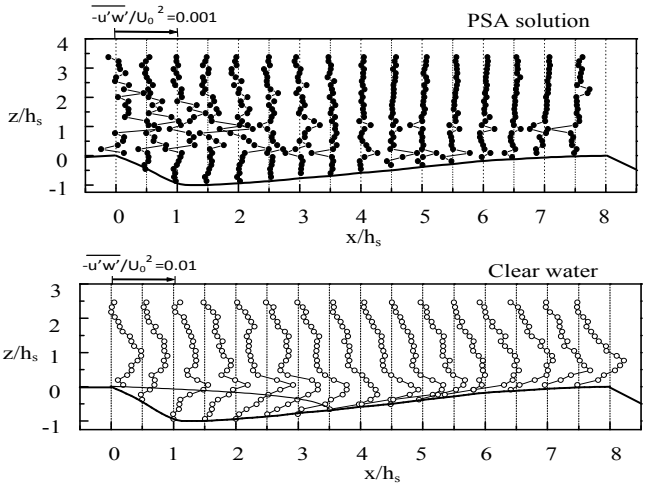

Figure 9. Vertical distribution of Reynolds stress

Figure 9 shows spatial changes in Reynolds shear stress. Overall, the maximum value for Reynolds in the PSA800mg/l case it is approximately less than 10% of that of the clear water. This corresponds to the decrease in turbulence intensity. In the clear water case, large values were shown near the point of inflection of main flow velocity and in the region downstream of the reattachment point, near the bed surface. PSA solution in both viscosity levels demonstrated close to 0 value near the reattachment point at x/hs=3.5~4.5. In the deceleration region between the ridge to the point of x/hs=3.5, the positive maximum value was attained. In the acceleration region from x/hs=5 to the downstream ridge, the negative maximum value was reported. This suggest that turbulence caused by flow separation from the crest was reduced in the flow direction, and momentum transport and energy losses due to turbulence decreased as the viscosity of the PSA solution increased. In particular, turbulence intensity and energy losses due to turbulence were very small in the PSA 800 mg/l solution case in which the resistance coefficient reached the maximum value.

Shear rate and shear stress

Figure 10 illustrates the rate of change for the vertical distribution of the main flow velocity in the vertical direction.

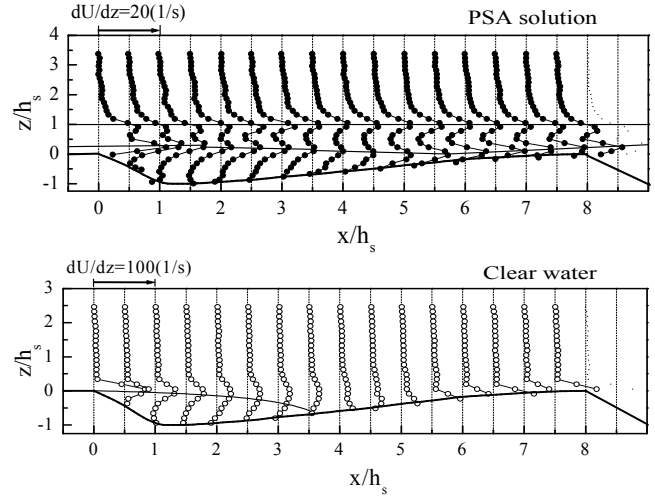

Figure 10. Vertical distribution of shear rate

The rate of change for main flow velocity in the vertical direction was in the range of: 0-20(1/s) in the PSA 800mg/l case and 0-100(1/s) in the clear water case. Compared to the clear water case, the rate of change for main flow velocity was lower in the PSA solution cases due to the effects of viscosity. In the PSA800mg/l solution case, the maximum value for turbulence intensity was identified at two points: z/ h_s=1 and z/h_s=0.2¤0.3, respectively.

Figure 11 shows the spatial distribution of viscous stress in PSA solutions (C_w=800 mg/l). Based on the power-law model, viscous stress is determined by Eqs. (3) and (4):

$$\tau_\mu = \mu\left(\frac{dU}{dy}\right) \quad (3)$$

$$\mu = \eta_0\left(\frac{du}{dz}\right)^{n-1} \quad (4)$$

The apparent viscosity coefficient is represented by μ, and the experimental values of η_0 and the exponent n were determined by least-squares approximation of the experimental data. Viscous stress demonstrated similar trends as those for spatial distribution of turbulence intensity and shear rate.

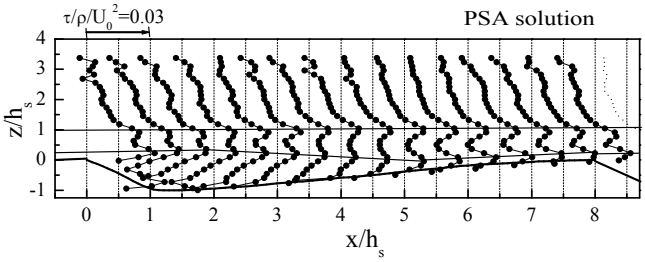

Figure 11. Vertical distribution of viscous stress

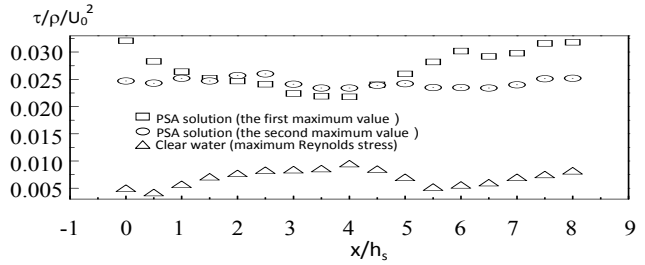

Figure 12. Streamwise distribution of maximum shear stress

Figure 12 describes the distribution of shear stress. Shear stress can be calculated from Eq.(5):

$$\tau = -\rho\overline{u'w'} + \mu\left(\frac{du}{dz}\right) \quad (5)$$

Change in vertical distribution of the shear stress in the flow direction demonstrated the intermittency similar to the one observed in spatial distribution of the turbulence intensity in the vertical direction. In the PSA 800mg/l solution case, the maximum value occurring near z/hs = 0.2 to 0.3 is referred to as the first maximum value, and the maximum value occurring near z/hs=1 is referred to as the second maximum value.

In the PSA800mg/l solution case, the first maximum value of shear stress becomes small near the reattachment point, and the second maximum value does show notable change throughout the wave

length section. In addition, the values are about 2.2 to 7 times as large in the PSA 800mg/l solution case than in the clear water case. Resistance to fluid constitutes: (1) viscosity shear stress caused by viscosity and (2) Reynolds shear stress caused by turbulence. The reasons why the total resistance coefficient decreased up to 27% compared to the clear water case in the PSA 400 mg/l case (7% sediment concentration) with the increase in the concentration of the PSA solution, a non-Newtonian fluid, might be attributed to: (1) the increase in the concentration associated with the viscosity was reduced in the flow direction by the turbulence caused by flow separation from the crest and (2) the decrease in momentum transport and energy losses due to turbulence. The total resistance coefficient tended to increase again in the solution with the concentration level higher than the PSA 400mg/l. Another reason for why the total resistance coefficient increased about 146% of the clear water case in the PSA 800mg/l (10% sediment concentration) case might be that despite the decrease in momentum transport, energy losses caused by viscosity became prominent.

CONCLUSIONS

In this study, sodium polyacrylate (PSA) solution that is similar in viscosity characteristics to high-concentrated sediment flows was used to clarify the resistance characteristics and flow mechanism of high-concentrated sediment flows over a dune type bed. Specifically, we applied the Particle Image Velocimetry measurement system to compare the high-concentrated sediment flows to the clear water flows. The results are summarized in the following six points.

1. The kinematic viscosities of PSA solutions having concentrations of 300 mg/l, 400 mg/l, 500 mg/l and 800 mg/l show non-Newtonian fluid properties similar to the kinematic viscosities of kaolin suspensions having volumetric concentrations (C_v) of 6%, 7%, 8% and 10%, respectively.
2. The total resistance coefficient Cf decreased to PSA400mg/l (7% sediment concentration) with the increase in the PSA solution concentration, up to 27% compared to that of clear water and tended to increase again from that point. In the PSA800mg/l case (10% sediment concentration) the resistance increased about 146% of that of the clear water.
3. Unlike in the clear water flow, flow separation and the circulating flow formed by flow separation were not noteworthy in the high viscosity PSA solution case, and the two regions with high levels of shear rate were identified at z/h_s=1and z/h_s=0.2 ~0.3.
4. Compared to the clear water case, in the PSA 800mg/l solution case, turbulence intensity decreased to about 50% in the streamwise direction and about 30% in the vertical direction. The location of the maximum value of turbulence intensity in the PSA solution showed close agreement with the location of the maximum value of the shear rate, but the spatial distribution differed considerably from that in the clear water. The maximum value for Reynolds stress corresponds to the decrease in the maximum value for turbulence intensity. In the PSA800mg/l case, it is approximately less than 10% of that in the clear water.
5. The spatial distribution of viscous stress in the PSA solution showed a tendency similar to the tendencies of the spatial distributions of turbulence intensity and the shear rate. In the PSA800mg/l solution case, the first maximum value of shear stress became small near the reattachment point, and the second maximum value did not show notable change throughout the wave length section. In addition, the values of shear stress were about 2.2 to 7 times as large in the PSA 800mg/l solution case as in the clear water case.
6. One of the reasons for why the total resistance coefficient increased about 146% of the clear water case in the PSA 800mg/l (10% sediment concentration) case might be attributed to the fact that: despite the decrease in momentum transport, energy losses caused by viscosity was prominent.

REFERENCES

[1.] Bradley, J. B. and McCutcheon, S.C: The effect of high sediment concentration on transport processes and flow Phenomena, proc.Conf. Erosion, Debris prevention, Japan,1985

[2.] Coussot, P.: Rheology of debris flow-Study of concentrated suspensions. Ph.D.thesis, INPG, Grenoble, France, 1992

[3.] Dodge, D.W., and Metzner, A.B.: Turbulent Flow of Non-Newtonian System, A.I.Ch.E.J., Vol. 5, No.2, 1959

[4.] Hershey, H.C., and Zakin, J.L.: Existence of Two Type of Drag-reduction in Pipe Flow of Dilute Polymer Solutions, Ind.Eng.Chem.Fundamentals, Vol.6, No.23, p.381, 1967.

[5.] Egashira S.,Ashida K., Tanonaka S. And Sato T.: Studies on Mud Flow-Stress Structure-, Annuals, Disas. Prev.Res. Inst., Kyoto Univ. No.35, B-2, pp79-88,1992.

[6.] Metzner, A.B., and M.G. Park: Turbulent Flow Characteristics of Viscoelastic Fluid, J. Fluid. Mech., Vol.20, p.291, 1964.

[7.] Oldroyd, J.G.: A Suggested Method of Detecting Wall Effects in Turbulent Flow Thorough Pipes, in Proc. First Intern.Congr.on Rheol., pp.130-134, Vol.II, North Holland, Amsterdam, 1948.

[8.] Ohmoto T., Cui Z. and Kakihara Y.: On Rheology of Hyperconcentrated Sediment-laden Flow, Journal of Applied Mechanics, JSCE, Vol.7, pp979-986, 2004.

[9.] Wang H. and X. Fei,: The fluctuation of Bingham shear stress on hyperconcentrated flow in flowing conditions, Proc. of 4th Intern. Symp. on River Sedimetation,pp.198-205,(1989).

[10.] Yang, C.T. and X.Kong.: Energy Dissipation Rate and Sediment Transport, Journal of Hydraulic Reasearch, Vol.29, no.4, pp.457-474, 1991.

[11.] Yang, C.T.: Sediment Transport in the Yellow River , Journal of Hydraulic Engineering , Vol.122, 2004, pp237-244, 1996.

[12.] Z.Y.Wang: A study on debris flow surges, Hydraulic Engineering'93, Vol.2, American Society of Civil Engneers, New York,pp. 1616-1621, 1993.